



ELSEVIER

Contents lists available at ScienceDirect

Deep-Sea Research II

journal homepage: www.elsevier.com/locate/dsr2

Coastal connectivity in the Gulf of Maine in spring and summer of 2004–2009



Yizhen Li^a, Ruoying He^{a,*}, James P. Manning^b

^a Department of Marine, Earth, and Atmospheric Sciences, North Carolina State University, 2800 Faucette Drive, Raleigh, NC 27695, USA

^b National Oceanic Atmospheric Administration, Northeast Fisheries Science Center, 166 Water Street, Woods Hole, MA 02543, USA

ARTICLE INFO

Available online 31 January 2013

Keywords:

Gulf of Maine
Coastal circulation
Connectivity
Lagrangian PDFs
Interannual variability
Source and destination strengths

ABSTRACT

Coastal ocean connectivity associated with the Gulf of Maine (GOM) surface flows in spring and summer seasons of 2004–2009 is studied using surface numerical particle tracking based on realistic regional ocean circulation hindcast solutions. Seven initial particle release sites are selected in key gulf regions often affected by harmful algal (*Alexandrium fundyense*) blooms, including Massachusetts Bay, the western GOM coastal area, the eastern GOM coastal area, the Bay of Fundy, Wilkinson Basin, the Jordan Basin, and a region seaward of Penobscot Bay. Surface particles are released every 5 days between February 1st and August 1st in each year, and the variability in their trajectories on interannual time scales is quantified by Lagrangian probability density function calculations. Coastal connectivity is further quantified using a connectivity matrix, identifying source and destination functions. Our results suggest that the interannual variability in coastal connectivity has strong impact on the spatial distribution of *A. fundyense* blooms in each year.

© 2013 Elsevier Ltd. All rights reserved.

1. Introduction

The Gulf of Maine (GOM) is a semi-closed marginal sea off the U.S. northeast seaboard. While the mean circulation in the gulf is known to be cyclonic (Bigelow, 1927; Lynch et al., 1997), significant seasonal and interannual variations in coastal current and transport have been identified by previous observational and modeling work (e.g., He and McGillicuddy, 2008; Manning et al., 2006, 2009; Pettigrew et al., 2005; Xue et al., 2000). For instance, there is strong continuity between the eastern Maine Coastal Current (EMCC) and western Maine Coastal Current (WMCC) in certain years (e.g., 2000 and 2003), as opposed to a more disrupted coastal flow structure in other years (e.g., 1998 and 2002) when the EMCC veers offshore southeast of Penobscot Bay (Pettigrew et al., 2005; Xue et al., 2008). Further north, the Bay of Fundy water typically has high self-retentiveness, but significant interannual variability has been observed in the rate at which BOF waters leak into the EGOM through various exit pathways (Aretxabaleta et al., 2008, 2009). Offshore, the Jordan Basin gyre that tends to intensify in the summer season (Beardsley et al., 1997; Brooks, 1985) is clearly also influenced by offshore and upstream forcing variations on interannual time scales.

A major research focus in the GOM is the dispersion of planktonic species by the Gulf of Maine circulation. Hannah et al. (1998) used a model-generated climatological mean circulation to study the upper-ocean transport mechanisms for the copepod *Calanus finmarchicus*, which is a keystone species of the annual zooplankton bloom in the GOM. Their results showed that the southward surface Ekman drift induced by northwesterly wind can act as a conveyor belt, transporting *C. finmarchicus* from the GOM to the Georges Bank in winter and spring seasons. A recent study by Xue et al. (2008) focused on the early life stage of lobsters in the GOM. They coupled a realistic circulation hindcast model (the Princeton Ocean Model) with an individual based biological model that considered lobster egg production, temperature-dependent larval growth, and stage-specific vertical distributions. Numerical lobster larvae were released three times each month from June to September near shore (within the 100-m isobath). Results showed relatively lower accumulations of early stage lobsters along the eastern Maine coast than along the western Maine coast. Using the same model setup, the study of Incze et al. (2010) further included mortality in the individual based biological model and focused on the relative contributions of different source regions to the distribution of postlarvae along the coastal zone. A connectivity matrix was constructed to show that connections between different coastal locations have strong interannual variability in postlarval abundance in response to circulation and temperature variations. Manning and Churchill (2005, 2006) and Manning et al. (2009) described drifter

* Corresponding author. Tel.: +1 919 513 0249.
E-mail address: rhe@ncsu.edu (R. He).

dispersion studies in the GOM. The latter work in particular utilized observed drifter trajectories collected from 1988 to 2007 to describe the Maine Coastal Current (MCC) and the coastal transit time along different isobaths.

A statistically-based Lagrangian PDF (LPDF) method was introduced by Mitarai et al. (2009) to describe the probability density function of particle displacement and coastal connectivity in the Southern California Bight (SCB). Driven by simulated ocean currents, their ensemble numerical particle dispersal patterns exhibited a strong dependence on the initial release locations and advection time scales being studied. Moreover, pronounced dispersion variability on seasonal to interannual timescales was shown to be largely determined by eddy activity and synoptic wind-forcing variations in the SCB. Based on the connectivity matrix, the source and destination strengths were computed to quantify the degrees of connection between different coastal locations selected in their study.

Inspired by drifter observation studies (e.g., Manning et al., 2009) in the Gulf of Maine, we intend to further analyze the coastal Lagrangian connectivity using numerical particle tracking and the LPDF method described by Mitarai et al. (2009). Our key scientific motivation is to better understand the role of ocean circulation in affecting the harmful algal bloom (*Alexandrium fundyense*) distributions on interannual time scales. Early studies (e.g., Anderson et al., 2005a; McGillicuddy et al., 2003, 2005b) have shown that *A. fundyense* cells are initiated by cyst germination in early spring of each year. The resulting blooms (of different intensity in each year) are present in various GOM coastal regions throughout the summer. Here we seek to understand how the coastal circulation variability influences bloom dispersion, which *A. fundyense* source location(s) are most important, and where their most likely destinations are located.

In Section 2 we provide a description of our GOM coastal circulation model, and a brief overview of coastal connectivity and LPDF concepts. Section 3 presents the model-data comparisons, GOM LPDF results, and connectivity matrix, source and destination function analyses. Section 4 discusses connectivity variability on interannual time scales and the possible driving mechanisms, followed by a summary and discussion in Section 5.

2. Methods

2.1. Hydrodynamic model, observations, and particle tracking tool

The GOM circulation hindcast was performed using a regional implementation of the Regional Ocean Modeling System (Haidvogel et al., 2008; Shchepetkin and McWilliams, 2005). ROMS is a free-surface, hydrostatic, primitive-equation model that employs split-explicit separation of fast barotropic and slow baroclinic modes and vertically stretched terrain-following coordinates. We implemented a multi-nested configuration consisting of circulation downscaling from a global data assimilative Hybrid Coordinate Ocean Model (HYCOM/NCODA) to a shelf-wide ROMS model, and subsequently to the GOM ROMS model (He et al., 2008). The global HYCOM (<http://hycom.rsmas.miami.edu/dataserver>) assimilates satellite observed sea surface temperature and height, and ARGO measured temperature and salinity profile data, providing daily data assimilative global circulation at about 10 km resolution. Inside HYCOM we have embedded a shelf-scale ROMS model that encompasses both the Mid-Atlantic Bight (MAB) and GOM (hereafter MABGOM ROMS) via a one-way nesting approach. Horizontal resolution of MABGOM ROMS is 5(10) km in the across- (along-) shelf direction. Vertically there are 36 terrain-following levels in the water column with higher resolution near the surface and bottom to better resolve boundary layer dynamics. For the purpose of one-way nesting,

MABGOM ROMS open boundary conditions (OBCs) were applied to temperature, salinity, and baroclinic velocity following the method of Marchesiello et al. (2001), whereby Orlandi-type radiation conditions were used in conjunction with relaxation. Free surface and depth-averaged velocity boundary conditions were specified using the method of Flather (1976) with the external values provided by HYCOM. Because HYCOM solutions do not include tides, tidal harmonics (M_2 , S_2 , N_2 , K_2 , K_1 , O_1 and Q_1) from an ADCIRC simulation of the western Atlantic (Luettich et al., 1992) were superimposed. Analysis of the interior solution confirmed this approach yielded accurate tidal predictions, similar to earlier results (e.g. He et al., 2008; Moody et al., 1984; Xue et al., 2000). Mellor and Yamada (1982) closure scheme was applied to compute the vertical turbulent mixing, as well as a quadratic drag formulation for specification of bottom friction. The same one-way nesting approach and OBC treatment were used to downscale the shelf-scale MABGOM circulation to the inner-most GOM model. The GOM ROMS has a spatial resolution of 1 (3)-km in the across-shelf (along-shore) direction, and also has 36 vertical layers. This multi-nested downscaling configuration enables the high-resolution GOM ROMS to achieve numerically accurate and dynamically consistent boundary forcing from its large-scale “parent” model. As earlier studies (e.g., He et al., 2005) have shown, significant skill improvement in modeling GOM hydrography and transport can be achieved by using more accurate OBCs specifications.

Surface atmospheric forcing parameters used in our regional ROMS simulations, including cloud fraction, precipitation, surface pressure and humidity, air temperature, surface wind, and short-wave radiation were obtained from the National Center for Environmental Prediction (NCEP), North America Regional Reanalysis (NARR). Spatial and temporal resolutions of these forcing fields are 32-km and 3 h, respectively. They were applied in the standard bulk flux formulation to derive wind stress and net surface heat flux needed by the simulations. To further constrain the surface heat flux, we also followed the same approach used in He and Weisberg (2003) to relax the modeled SST field to NOAA Coast Watch daily, $1/10^\circ$ cloud-free SST product with a timescale of 0.5 day. The GOM ROMS circulation model has been coupled with an *A. fundyense* population dynamics model to simulate the circulation and harmful algal blooms in different years. Interested readers are referred to He et al. (2008), Li et al. (2009), and McGillicuddy et al. (2011) for a more detailed description of that coupled biophysical model.

In-situ observations used in this study include time series of wind and ocean currents measured by moorings of the Gulf of Maine Ocean Observing System (now part of the Northeast Coastal Ocean Observation System NERACOOS, <http://www.neracoos.org>), e.g., Pettigrew et al., 2011), and the long-term drifter statistics provided by Manning et al. (2009).

The numerical surface particle trajectories were calculated using the Larval Transport model (LTRANS; North et al., 2006a, 2006b, 2008; Schlag et al., 2008), which is an offline particle tracking model that runs with GOM ROMS simulated surface current archives. Our objective is to understand the transport pathways of vegetative *A. fundyense* cells at the ocean surface. As such, numerical particles are ‘drogued’ at 1-m (isobaric) and are not impacted by the vertical velocity. LTRANS model tracking includes a 4th-order Runge–Kutta scheme for advection. In this study, we also activated the random displacement module to mimic sub-grid scale turbulent diffusion. To avoid possible beaching (hitting the land-sea boundary) of the particles, a reflective horizontal boundary condition was applied. That is once a particle hits the land boundary, it is reflected back using the same angle it had approaching the boundary, so particles are kept within the model domain.

We selected a set of particle release domains in the GOM (Fig. 1), including seven sites in Massachusetts Bay (MA, sites 1–7),

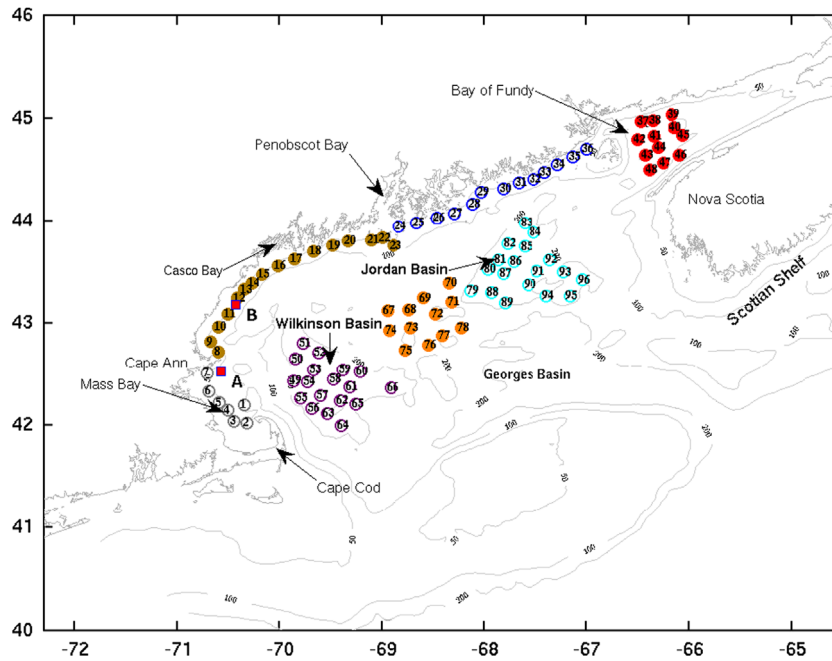


Fig. 1. Locations of seven particle release regions in the Gulf of Maine, which include Massachusetts Bay (MASS, in gray), the western Gulf of Maine (WGOM, in brown) coastal area, the eastern Gulf of Maine (EGOM, in blue) coastal area, the Bay of Fundy (BOF, in red), Wilkinson Basin (WK, in purple), Jordan basin (JB, in orange), and the area offshore of Penobscot Bay (OFFPB, in cyan). For each site, the initial release points are chosen based on a 6-km radius circular area. Red rectangular symbols represent the locations of NERACOOS buoys A and B. Also shown are the coastal bathymetric contours (50 m, 150 m, and 200 m), and other important geographic sites in the GOM.

16 sites in the western GOM (WGOM, sites 8–23) coastal area, 9 sites in the eastern GOM (sites 24–36, EGOM) coastal area, 12 sites in the Bay of Fundy (BOF, sites 37–48), 18 sites in Wilkinson Basin (WK, sites 49–66), 12 sites in a region seaward of Penobscot Bay (OFFPB, sites 67–78) and 18 sites in Jordan Basin (JB, sites 79–96). Following the same approach used by [Mitarai et al. \(2009\)](#), each site covers a 6-km radius circular area rather than just a single point in the ocean. Among these sites, BOF, OFFPB, and JB are known to be important cyst germination (“source”) locations for *A. fundyense* blooms (e.g., [Anderson et al., 2005a](#)). Sites 8–23 and sites 24–36 are centered along the 50-m isobaths in the EGOM and WGOM coastal areas respectively, and are approximately 12-km offshore of the coastline. Therefore these 6-km radius circular areas cover most of shelf regions, and are among those “destination” regions where repetitive *A. fundyense* blooms are often observed and shellfish bed closures enforced ([McGillcuddy et al., 2005a](#)).

We focused on the subtidal transport in spring and summer seasons, and for this purpose, surface particle trajectories were computed by LTRANS using the sub-tidal (12.42 h averaged) surface velocity simulated in each year from February 1st to August 1st in 2004–2009. The M_2 tidal averaging procedure ignores other tidal constituents; the effect of the residual tidal constituents will be discussed in [Section 4](#). A total of 1531 particles were released every 5 days over 6-year study period within the 6-km radius of each of these sites, resulting a total of 19,841,760 particle trajectories, which were used to quantify connections among GOM coastal regions that have been chosen in this study.

2.2. Lagrangian PDFs

Following [Mitarai et al. \(2009\)](#), we can define the Lagrangian Probability Functions (LPDFs) as the probability density of particle displacement. For a given advection time scale τ , sampling space variable ε , initial position a , and the position of n -th particle

$X_n(\tau, a)$, the discrete representation of LPDFs $f'_X(\varepsilon; \tau, a)$ is defined as

$$f'_X(\varepsilon; \tau, a) = \frac{1}{N} \sum_{n=1}^N \delta(X_n(\tau, a) - \varepsilon) \quad (1)$$

where N is the total number of Lagrangian particles, and δ is the Dirac delta function. The Dirac function is defined as the Heaviside function H in a unit area (i.e., $\delta = dH/dx$), where the Heaviside function H is typically known as the unit step function, such that

$$H(x) = \begin{cases} 0 & \text{if } n < x \\ 1 & \text{if } n \geq x \end{cases}$$

where n is the integer (grid number) along the directional axis x . As such, f'_X is also in units of reciprocal area.

The discrete LPDF f'_X can be expressed as spatially-averaged LPDFs over the surrounding area of each release site, that is

$$f'_X(\varepsilon; \tau, a) \approx \frac{1}{\pi R^2} \int_{|r| \leq R} f'_X(\varepsilon; \tau, a+r) r dr \quad (2)$$

where R is the radius of each release site (taken as 6-km in this study). A smooth operator (Gaussian filter with radius of 6 km) was then applied to remove subgrid-scale noise to get the LPDF f_X .

Based on the LPDF, the coastal connectivity $C_{j,i}$ is then defined as the probability of a water parcel that moves from source j to destination i over a time interval τ . For a given set of source location x_j and a destination location x_i , the value of $C_{j,i}$ is evaluated from the LPDF as

$$C_{j,i}(\tau) = f_X(\varepsilon = x_i; \tau, a = x_j) (\pi R^2) \quad (3)$$

The connectivity matrix can be normalized by the surrounding area πR^2 of each release site to convert probability densities into probabilities.

Once we have the connectivity matrix, the destination strength $D_i(\tau)$, representing the relative ‘attractiveness’ of site i for all Lagrangian particles released in the study domain over

a release time τ , can be calculated by summing the connectivity matrix over all source sites in the domain, i.e.

$$D_i(\tau) = \sum_{j \in J} C_{j,i}(\tau), \quad J = j_1, j_2, \dots, j_N \quad (4)$$

In other words, this quantity represents where the particles from different source sites are traveling to.

Similarly, the source strength $S_j(\tau)$ measuring the relative success of particles moving from site j to other places in the domain within an advection time scale τ , can be calculated by summing the connectivity matrix over all destination sites in the study domain. Similarly, the source strength $S_j(\tau)$ measuring the relative success of particles moving from site j to other places in the domain within an advection time scale τ , can be calculated by summing the connectivity matrix over all destination sites in the study domain as

$$S_j(\tau) = \sum_{i \in I} C_{j,i}(\tau), \quad I = i_1, i_2, \dots, i_N \quad (5)$$

In other words, this quantity represents where the particles arriving at a certain destination are coming from.

3. Results

3.1. Validation of circulation model

Because the utility of the simulated particle trajectories is based on the quality of ocean current simulation, extensive model-data comparisons have been performed to gauge the performance of the GOM regional ocean circulation model. Examples of model skill assessment on synoptic to seasonal time scales were given in [He](#)

[et al. \(2008\)](#), which compared the model hindcast solutions in 2005 with observed sea-level, currents, surface temperature and salinity; and in [Li et al. \(2009\)](#), which compared model solutions with a similar set of observations in the 2006. All results suggested that the GOM ROMS model can reasonably capture observed hydrographic and circulation variability.

In this study additional validations were made between simulated and observed monthly mean surface currents over the 6-year period, showing the model has reasonably good skill in reproducing low-frequency circulation variability. Taking the comparisons against velocity observation at GoMOOS moorings A and B for example ([Fig. 2](#)), we see the model generally reproduced the observed flow patterns as indicated by complex correlation coefficients exceeding 0.5. In terms of mean velocity, the model underestimated (overestimated) observations at buoy A (B), as shown by an amplitude regression slope of 0.6 (1.1), respectively. The implication of the over-/under-estimation of the coastal currents on the particle trajectory simulation will be discussed in [Section 5](#).

[Manning et al. \(2009\)](#) derived a 0.5° GOM mean surface current field based on long-term drifter observations collected mainly in spring and summer seasons during the period 1988–2007. This dataset provided another means for validating model simulated surface current fields. To do that, we averaged modeled surface velocity for the February–August period of 2004–2009 and remapped the resulting mean field from the ROMS model grid to the same $0.5^\circ \times 0.5^\circ$ drifter analysis grid ([Fig. 3](#)). While the sampling periods do not coincide exactly, the observed major GOM circulation features including the mean inflow from the Nova Scotia, the MCC, and the circulation on Georges Bank are all reasonably reproduced by the model. For each $0.5^\circ \times 0.5^\circ$ grid box, direct statistical comparisons on mean velocity speed and direction (shown by numbers inside each grid box) indicate the modeled

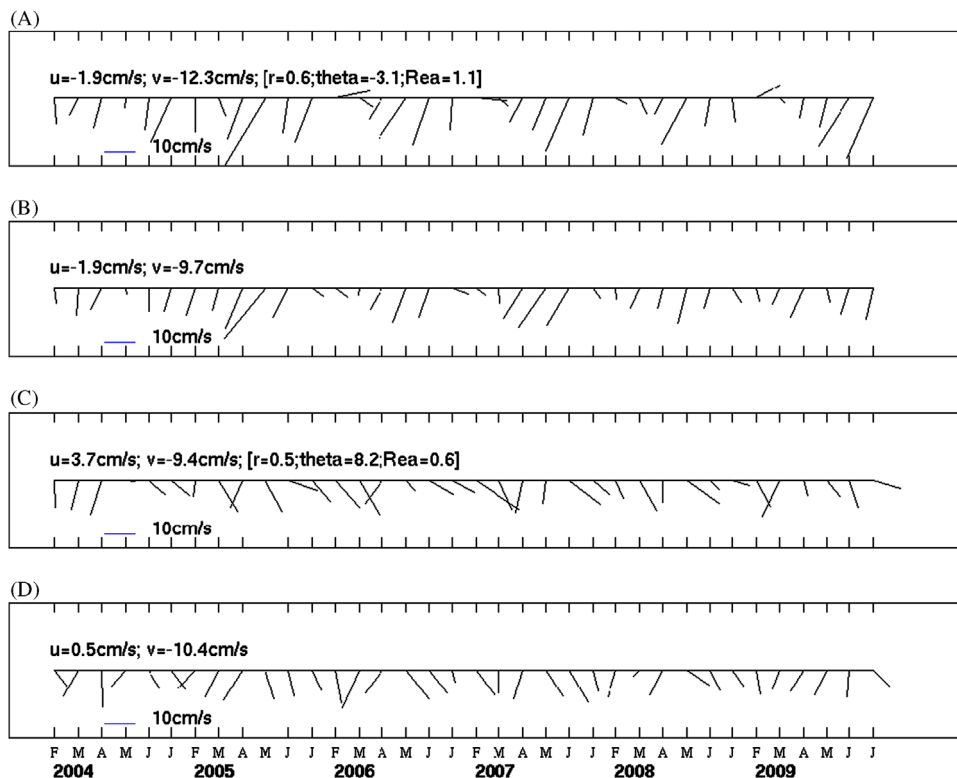


Fig. 2. Comparisons between modeled and observed monthly surface currents at buoy B (upper 2 panels) and at buoy A (lower 2 panels). Each vector current time series is accompanied by its mean east and north velocity components (left-hand couplet), and each model/data comparison is quantified by its complex correlation coefficient r , phase angle difference θ (angular deviation of the model vectors from the data vector measured counterclockwise), and amplitude regression slope Rea (right-hand triplet within the bracket). (A) Modeled surface current at Buoy B, (B) observed surface current at Buoy B, (C) modeled surface current at Buoy A, (D) observed surface current at Buoy A.

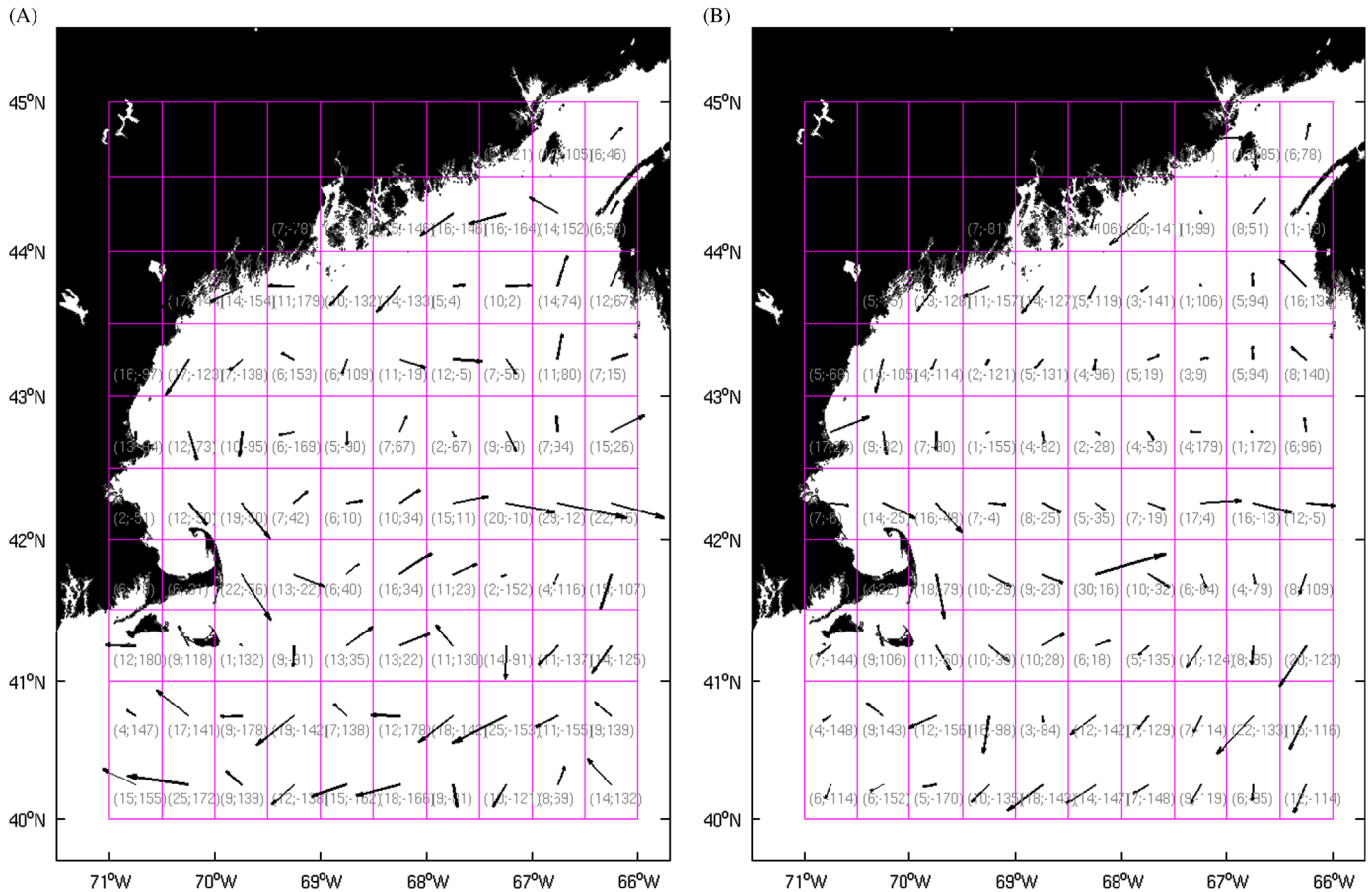


Fig. 3. Comparisons between (A) observed and (B) simulated mean surface currents (unit: cm s^{-1}). The observed surface currents are derived on a $1/2^\circ$ grid from long-term drifter data by Manning et al. (2009), whereas the modeled mean surface currents are derived by temporally averaging of regional model hindcast solutions from 2004 to 2009. Couplet inside each grid box indicates the mean current amplitude (cm s^{-1}) and direction (degrees True).

coastal current resembles its observational counterpart in most areas except in Jordan Basin where the model underestimates the current.

Both synoptic model/data comparisons presented in earlier studies (He et al., 2008; Li et al., 2009) and the long-term mean comparisons give us the confidence that the offline Lagrangian transport analysis is couched in a realistic GOM hydrodynamic setting.

3.2. Mean Lagrangian PDFs

Based on the particle releases over the 6-year period, we computed the mean LPDFs for the February–August period according to the formulation in Section 2.2. Depending on the length of the tracking period (advection time τ), the time-averaged LPDFs display different spatial structures. Taking the BOF releases for example (Fig. 4), strong retention is clearly shown in the case with a 10-day advection time, but the pattern becomes gradually more dispersed as τ increases. The mean LPDFs associated with the advection time of 40-day and 60-day are very similar. We note such a time scale (40–60 days) is the typical duration of harmful algal blooms in the Gulf, and Manning et al. (2009) also showed that the mean transit time for drifters to travel from the BOF to the Great South Channel (GSC) is less than 2 months. Therefore, the following analyses focus on results using 40 days as the advection time scale to understand and quantify the probability of particles being transported in various areas of the GOM.

3.3. Mean connectivity matrix, source and destination strength

Based on Eq. (3), the connectivity matrix can be quantified using the LPDFs for given destination and source locations, illustrating the degree to which any two sites among all possible location combinations are connected over a designated advection timescale. Fig. 5 shows the mean coastal connectivity matrix for advection times of 10 days, 20 days, 40 days, and 60 days, respectively. Consistent with our analysis in Section 3.3, the case using an advection timescale of 10 days (Fig. 5A) shows that self-connectivity dominates. There are clear connections between immediately adjacent locations, such as between the EGOM coastal area and the WGOM coastal area, between BOF and EGOM, and between the WGOM and Massachusetts Bay. The connectivity pattern becomes more spread as the advection time increases to 20 days (Fig. 5B), 40 days (Fig. 5C) and 60 days (Fig. 5D). Again, we note the connectivity pattern with 60-day as the advection time scale is similar to that of 40-day.

The connectivity matrix associated with 40-day as the advection time scale (Fig. 5C) shows some interesting features. For example, while the BOF releases show the strongest self-connectivity, these particles can leak out, and travel to almost all other GOM sites selected in this study. JB releases also show strong self-sustenance, although to a less extent compared to BOF releases. Particles from JB releases can travel to most of locations under study, with only small numbers of particles being transported to the WGOM coastal area, the EGOM coastal area, and Massachusetts Bay. To better quantify the connectivity among different release domains chosen in this study, the spatial distribution of

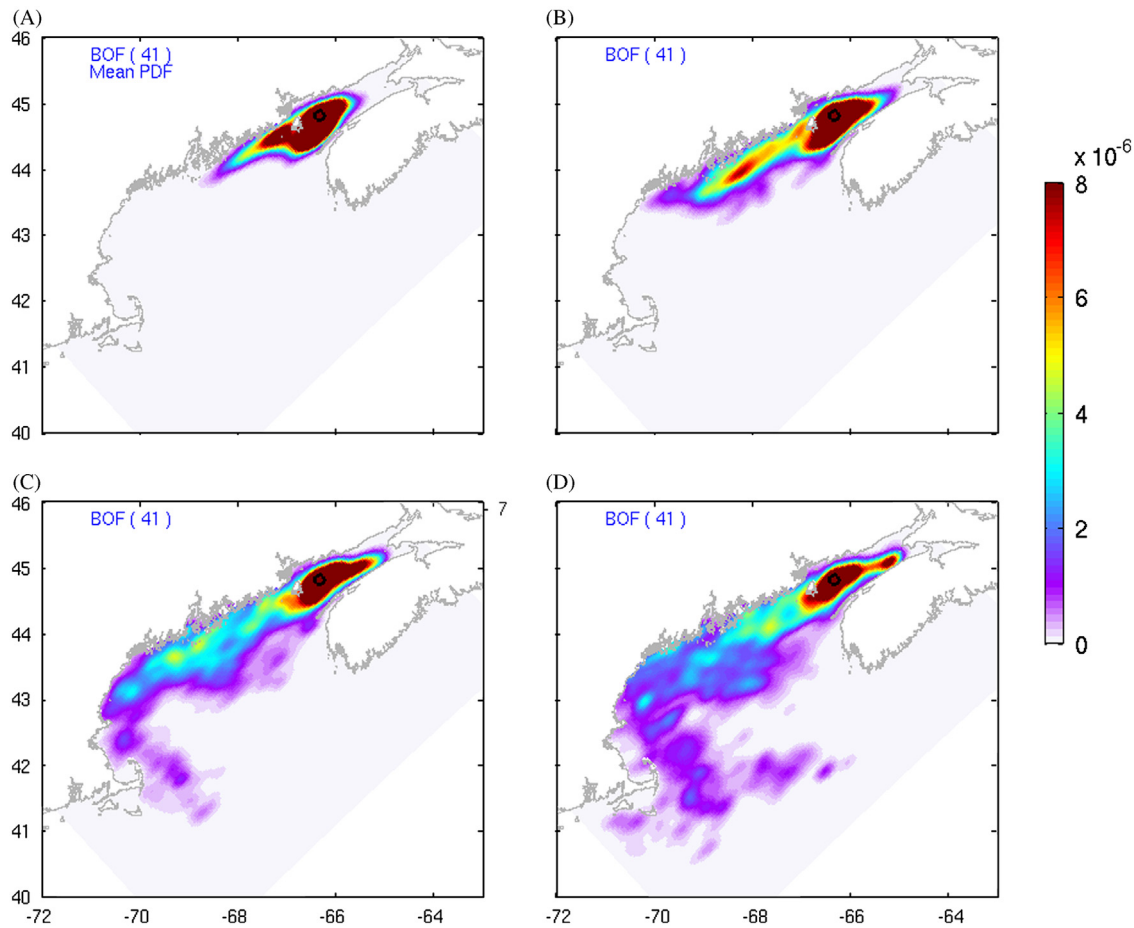


Fig. 4. Mean Lagrangian probability density functions (LPDFs) (unit: km^{-2}) for a single release site (site 41, as shown in Fig. 1) in the BOF based on the tracking with (A) 10-day, (B) 20-day, (C) 40-day, and (D) 60-day as the advection time.

source (Fig. 6) and destination (Fig. 7) strengths were calculated. To do that, the destination (source) strengths were computed according to Eqs. (4) and (5), and further normalized to indicate the percentage of the total released particles arriving at (originating from) each site.

The source strength functions show that (1) for particles that arrived at Massachusetts Bay sites (Fig. 6A), most of them are from the Massachusetts Bay sites themselves and the WGOM sites. Contributions from other sites decrease in the upstream direction; (2) for particles that arrived at the coastal WGOM sites, they are largely originated from coastal EGOM sites and BOF sites (Fig. 6B); (3) particles that arrived at the coastal EGOM sites (Fig. 6D) are almost entirely from BOF sites and (4) particles arrived at the BOF sites are nearly all from these sites themselves (Fig. 6C). At the offshore sites, particles that arrived at WK sites come from multiple sources (Fig. 6E) including BOF sites, EGOM sites, and JB sites. Particles transported to OFFPB (Fig. 6F) are from JB sites, OFFPB sites themselves, coastal EGOM sites and BOF sites. Particles traveled to JB sites (Fig. 6G) largely from with JB itself, plus some contributions from EGOM sites and BOF sites. If we consider all 96 selected release locations (in seven sub-regions) as a whole, BOF sites have the strongest source strength, suggesting particles released from BOF have the highest probability of arriving at the seven release regions being chosen in this study. We note these results are site specific. Other regions not considered in this study can also be effective sources. For example, it is known that water parcels from the Scotian shelf can travel to BOF and JB within a short time scale (e.g., Aretxabaleta et al., 2008).

The destination strength function represents the relative attractiveness of various sites being selected. It is clear that particles released from the MASS sites (Fig. 7A) cannot travel to other regions being considered in this study, as expected. Particles released from the WGOM sites (Fig. 7B) can spread to the MASS sites, WK sites, and some to OFFPB sites. Particles released from BOF sites travel primarily within the BOF sites (Fig. 7C), although some of them can flow downstream to both EGOM and WGOM sites. Particles released from EGOM sites (Fig. 7D) can travel to WGOM sites and MASS sites, but the majority go to offshore sites (JB, OFFPB, WK). In comparison, particles released from OFFPB (Fig. 7F) travel almost entirely among offshore sites (WK, OFFPB). Similarly, for particles released from JB (Fig. 7G), most of them are retained in JB. Some of them can travel to BOF and WK. If we consider all 96 destination locations from seven sub-regions we selected in this study (Fig. 7H), WK and BOF sites have the strongest destination strengths.

To summarize, among all the domains we have chosen, the BOF and JB are two strongest source regions, whereas WK and BOF are two most common destination regions. Overall, offshore sites have higher destination strength relative to the coastal sites.

4. Discussion

The connectivity matrix, source and destination strength functions presented in Section 3.3 represent long-term mean conditions. There is in fact strong temporal variability year by year. To quantify such variability, we computed the standard

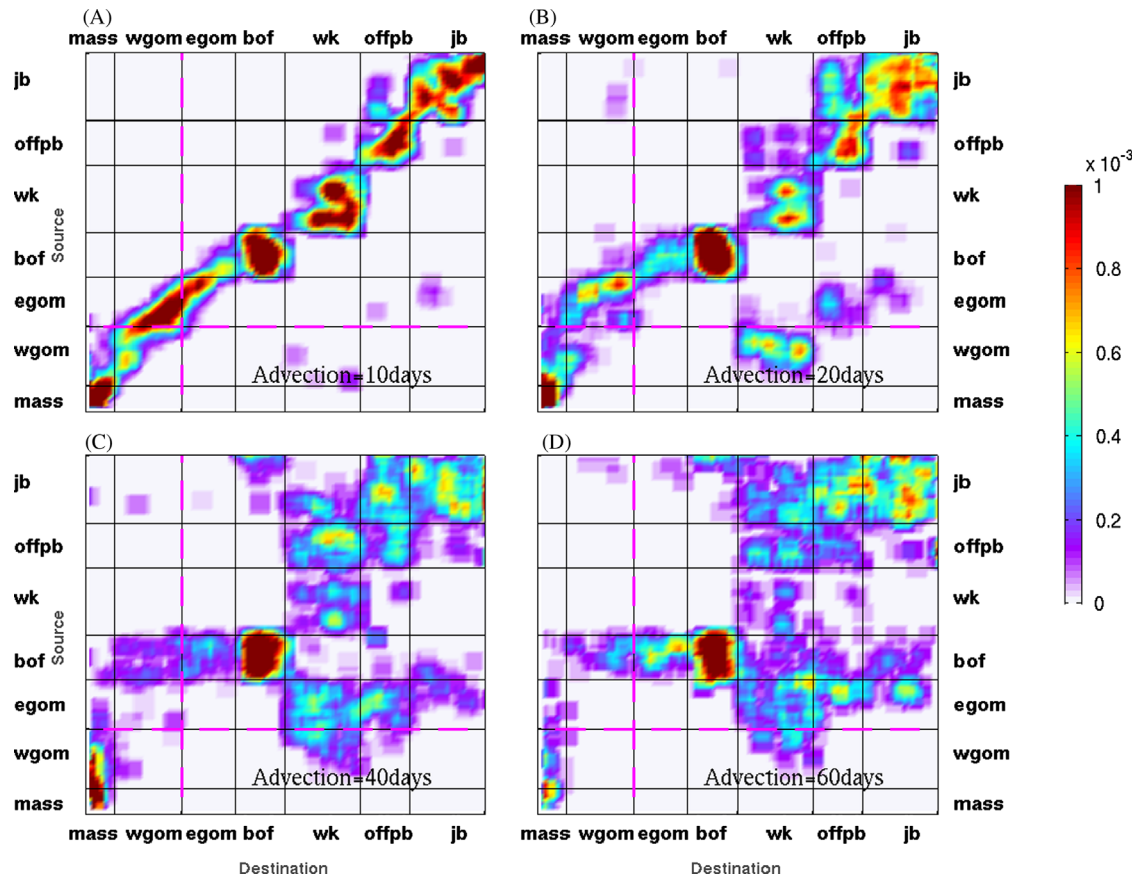


Fig. 5. Mean Gulf of Maine coastal connectivity matrix based on the particle tracking using (A) 10 days, (B) 20 days, (C) 40 days, and (D) 60 days as the advection time scale. The Y axis outlines each source location under study, whereas the X axis outlines each destination location under study. Both axes run from site 1 to site 96 as noted in Fig. 1. The connectivity matrices are normalized so that the summation of mean connectivity over all possible combinations is one. Pink dashed line indicates the borderline between eastern and western GOM sites. (For interpretation of the references to color in this figure legend, the reader is referred to the web version of this article.)

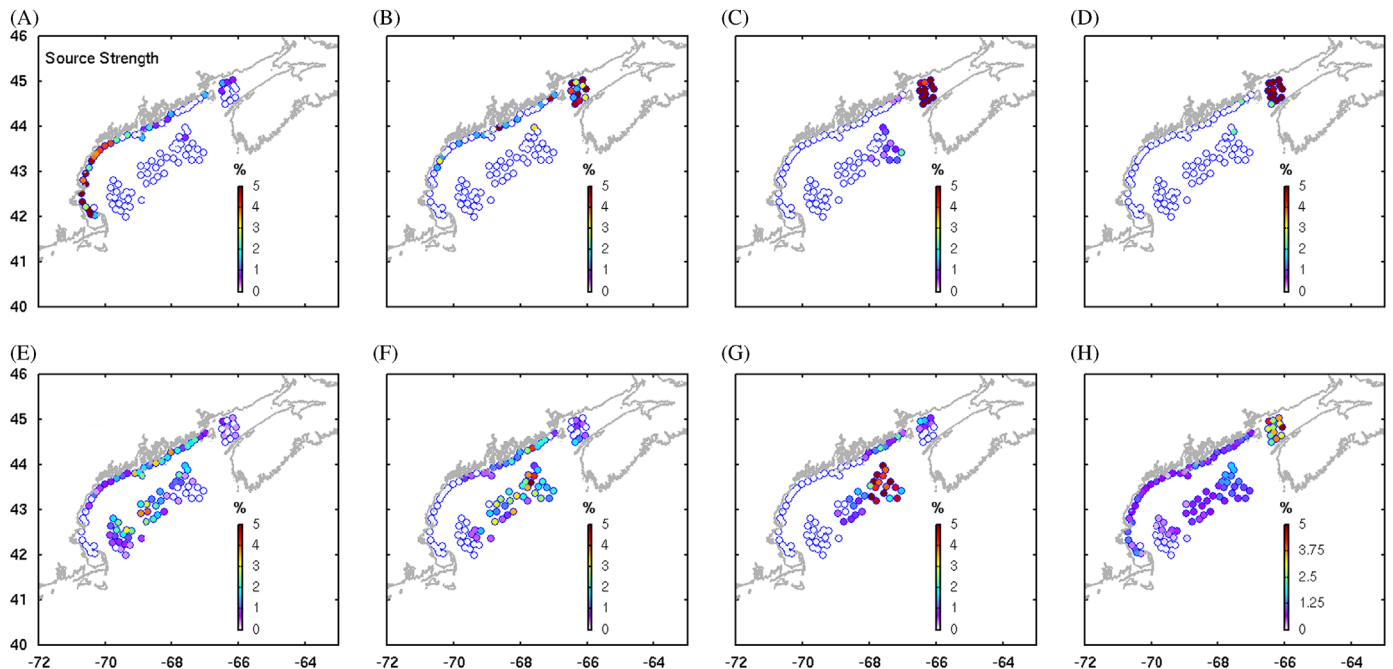


Fig. 6. Source locations and source strength functions of surface particles that are transported to (A) MASS, (B) WGOM coastal area, (C) BOF, (D) EGOM coastal area, (E) WK, (F) OFFPB, (G) JB, and (H) all sites in the GOM.

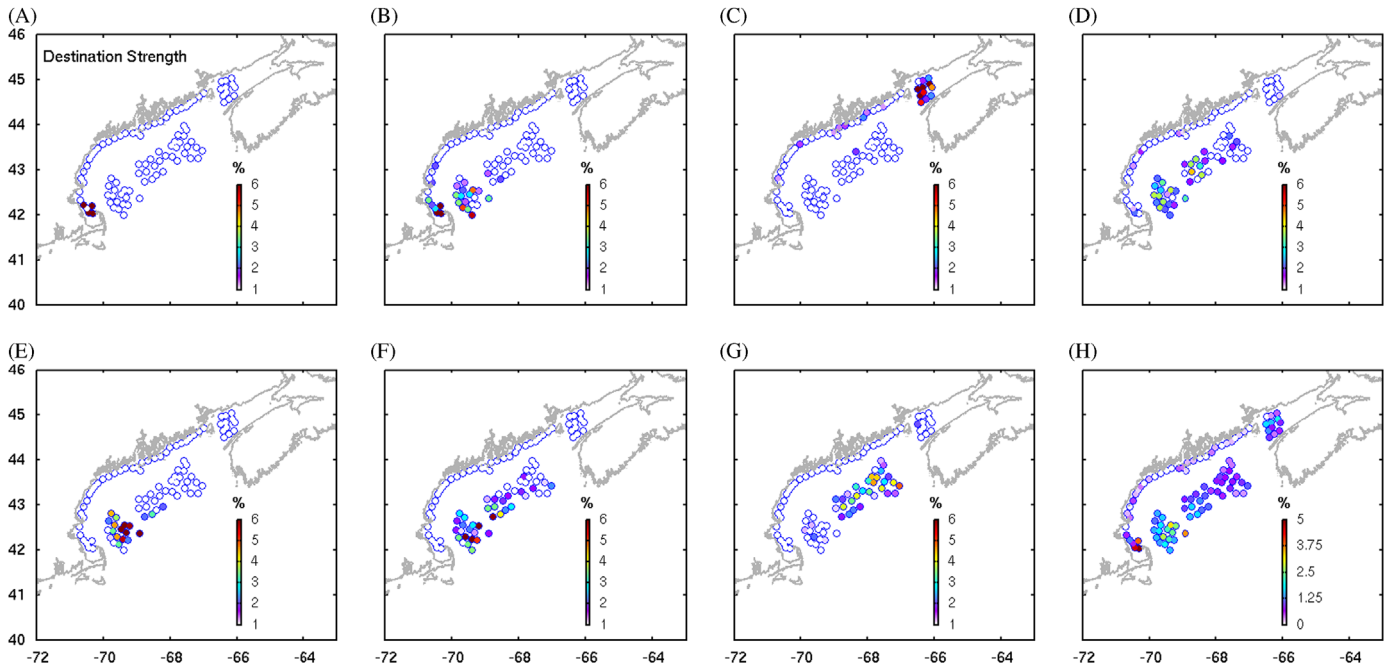


Fig. 7. Destination locations and destination strength functions of surface particles that are transported from (A) MASS, (B) WGOM coastal area, (C) BOF, (D) EGOM coastal area, (E) WK, (F) OFFPB, (G) JB, and (H) all sites in the GOM.

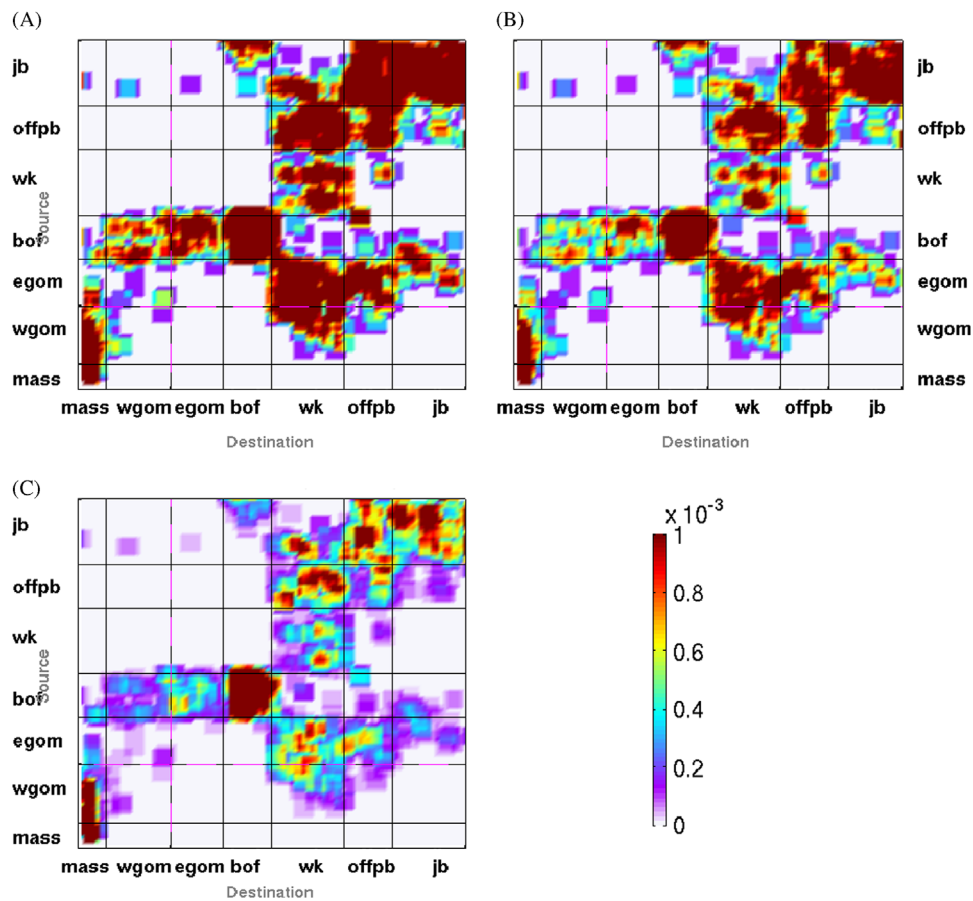


Fig. 8. (A) Standard deviation (STD), (B) low-frequency (seasonal and interannual) variability, and (C) intra-seasonal variability of the GOM connectivity matrix. Notation is the same as in Fig. 5.

deviation (STD) (Fig. 8A) relative to the mean over the 5-year period (2004–2009, Fig. 5C) examined in this study. The STD of the connectivity matrix shows substantial variability, highlighting

the varying and heterogeneous nature of the coastal circulation in each year. Following Mitarai et al. (2009), we temporally filtered the connectivity time series and calculated the root-mean

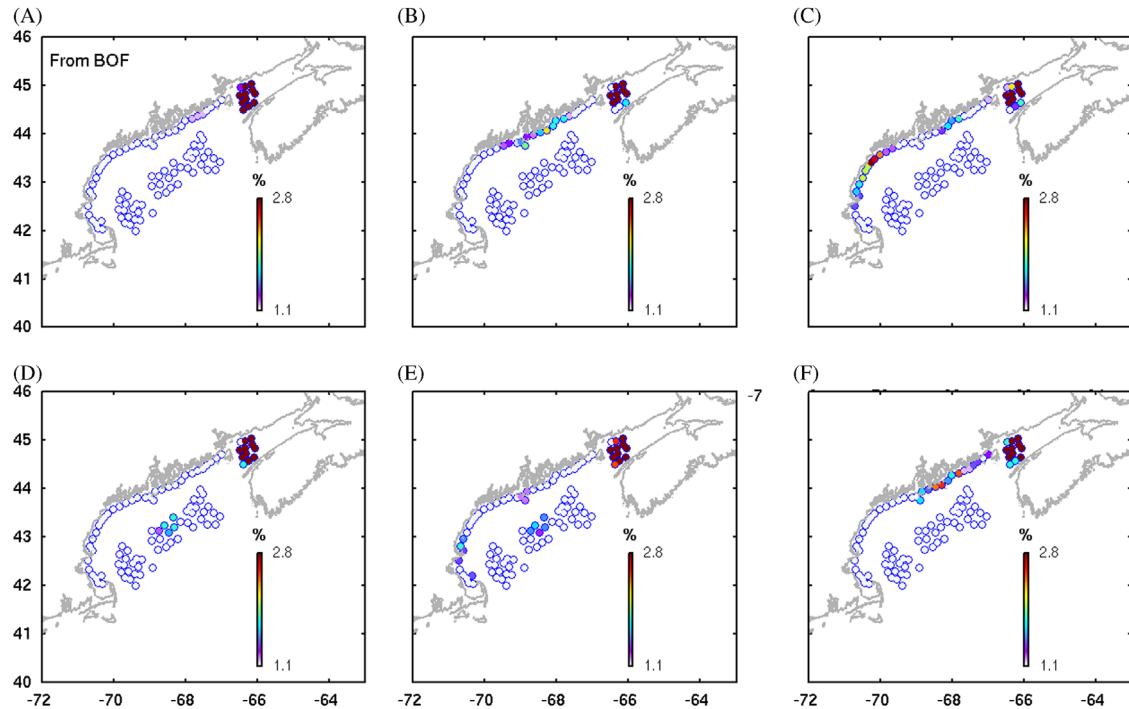


Fig. 9. Destination locations and strength functions of surface particles that are transported from the BOF in 2004–2009.

variance in the interannual and seasonal frequency bands (i.e., Fourier modes with time periods of 6-months or longer). The variability other than interannual- and seasonal-band were termed as ‘eddy-induced variability’ (Mitarai et al., 2009). By doing so, we separated the STD of connectivity into the interannual and seasonal low frequency part (Fig. 8B) and intra-seasonal eddy frequency variability (Fig. 8C).

We note that the seasonal and interannual variability (Fig. 8B) is three times larger than the mean (Fig. 5C), and dominates the connectivity variance. The higher frequency, eddy-driven variability is comparable to the mean, but much weaker than the lower-frequency seasonal and interannual signals, suggesting that in terms of the connectivity variations, the eddy-driven variability is a secondary factor. The interannual variability in connectivity can translate into significant modulations in transport pathways, and changes in source/destination function intensities. To further illustrate this aspect, we focused on particles released from the BOF, which is a major *A. fundyense* bloom incubator and cyst deposit site (Anderson et al., 2005b; Aretxabaleta et al., 2009; McGillicuddy et al., 2003). These particle trajectories clearly show rather different destination strength in each year between 2004 and 2009 (Fig. 9A–F). In 2004, particles released from our selected BOF sites stayed almost entirely within the BOF. In 2005, more particles traveled out of BOF to the coastal zone in the EGOM and near Penobscot Bay, suggesting retentiveness of the BOF gyre circulation became weaker compared to that in 2004. A similar situation occurred in 2006 and 2009, when we see a significant amount of particles traveled from BOF to WGOM (EGOM) coastal area in 2006 (2009), respectively. The BOF circulation returned to a more retentive stage in 2007 and 2008, and as a result, few particles were found outside the BOF. We note that the very strong connection between the BOF and the EGOM as indicated by the largest BOF particle destination strength in 2009 is coincident with extensive *A. fundyense* bloom and higher toxicity that occurred in summer 2009 along the Maine coast (McGillicuddy et al., 2014). Our results suggest that coastal connectivity and

transport may have played a key role in shaping the temporal and spatial distribution of the *A. fundyense* bloom, although the extent of toxicity extended into the WGOM, farther down the coast than indicated by the connectivity model. Along same line, the fact that more BOF particles traveled to WGOM (EGOM) sites in 2006 (2009) suggest the along shelf transport in 2006 was stronger than in 2009, and a flow discontinuity mechanism suggested by previous studies (Incze et al., 2010; Pettigrew et al., 2005; Xue et al., 2008) may be at work in 2009.

It should be noted that because our analysis focused on the connectivity variability on the interannual timescale, we used the M_2 tidal-period (12.42 h) averaged velocity field for all our particle tracking. This procedure essentially neglects the spring-neap cycle and other tidal constituents that still remain after the M_2 tidal period averaging. Analysis on this tidal residual effect on the coastal connectivity is needed in a future study. In addition, because of the finite spatial resolution of our circulation model (2–3 km), the coastal embayment and estuarine (e.g., Penobscot and Casco Bays) are not considered in our connectivity analysis. A higher resolution circulation hindcast and particle tracking simulation will be needed to resolve these regions. Another caveat that we alluded to earlier is that although our circulation hindcast reproduced the overall seasonal and interannual variability of coastal circulation (Fig. 2), the model overestimates the current amplitude at some locations (e.g., at buoy B) and underestimate currents at other locations (e.g. at buoy A). Such model errors will affect the particle tracking, leading to errors in the matrix. A more accurate representation of coastal circulation and transport requires an advanced data assimilative modeling approach, which is the subject of ongoing research that will be reported in future correspondence. Finally, while we are using distributions of numerical particles to infer *A. fundyense* bloom transport and spreading in the Gulf, we did not vary the particle release densities according to the *A. fundyense* cyst abundance (and hence the bloom limitation potential) at different sites being selected in this study. Model sensitivity experiments on the particle release

density, similar to what Incze et al. (2010) explored, is needed in a future study.

5. Conclusions

The Gulf of Maine coastal ocean connectivity in spring and summer seasons of 2004–2009 were studied using numerical surface particle trackings driven by realistic regional ocean circulation hindcast solutions. Our scientific motivation is to better understand the role of ocean circulation in affecting material property (such as harmful *A. fundyense* bloom) distributions in the GOM on inter-annual time scales. Early studies (e.g., Anderson et al., 2005a; McGillicuddy et al., 2003) have shown that *A. fundyense* cells are initiated from cyst germination in several sub-regions in the GOM in early spring, and subsequently dispersed by coastal current to other areas in the gulf. Mean LPDFs confirm conventional understanding on the climatological mean circulation and transport patterns in the GOM, including the MCC, BOF gyre, and Jordan Basin Gyre. The connectivity matrix shows that among the coastal sites selected in this study the BOF and JB are two strongest source regions in the GOM, whereas WK and BOF are two destination regions having the most “attractiveness”. Offshore sites have higher destination strengths relative to the coastal sites. Significant interannual variability is also seen in LPDFs. The BOF particles have the strongest destination strength at the EGOM coastal area in spring and summer 2009. This coincides with the observed strong *A. fundyense* bloom and toxicity concentrations in that area in June/July 2009, suggesting an important linkage between coastal transport and bloom distribution.

Acknowledgments

We thank the Northeastern Regional Association of Coastal Ocean Observing Systems (NERACOOS) for providing the mooring data used in this study. We are grateful to Drs. S. Mitarai, D. Siegel and P. Niiler for their helpful discussions on the concepts of LPDFs and eddy diffusivity. Research supports provided by the National Oceanic Atmospheric Administration (grant NA06NOS4780245) through the ECOHAB-GOMTOX program are greatly appreciated. This is ECOHAB contribution number 728.

References

- Anderson, D.M., Keafer, B.A., McGillicuddy, D.J., Mickelson, M.J., Keay, K.E., Libby, P.S., Manning, J.P., Mayo, C.A., Wittaker, D.K., Hickey, J.M., He, R., Lynch, D.R., Smith, K.W., 2005a. Initial observation of the 2005 *Alexandrium fundyense* bloom in the southern New England: general patterns and mechanisms. *Deep-Sea Res. II* 52, 2856–2876.
- Anderson, D.M., Stock, C.A., Keafer, B.A., Bronzino Nelson, A., Thompson, B., McGillicuddy, D.J., Keller, M., Matrai, P.A., Martin, J., 2005b. *Alexandrium fundyense* cyst dynamics in the Gulf of Maine. *Deep-Sea Res. II* 52 (19–21), 2522–2542.
- Aretxabaleta, A.L., McGillicuddy, D.J., Smith, K.W., Lynch, D.R., 2008. Model simulations of the Bay of Fundy Gyre: 1. Climatological results. *J. Geophys. Res.* 113, C10027, <http://dx.doi.org/10.1029/2007JC004480>.
- Aretxabaleta, A.L., McGillicuddy, D.J., Smith, K.W., Manning, J.P., Lynch, D.R., 2009. Model simulations of the Bay of Fundy Gyre: 2. Hindcasts for 2005–2007 reveal interannual variability in retentiveness. *J. Geophys. Res.* 114, C09005, <http://dx.doi.org/10.1029/2008JC004948>.
- Beardsley, R.C., Butman, W.R., Geyer, P., Smith, 1997. Physical oceanography of the Gulf of Maine: An update. In: Wallace G.T., Braasch E.F. (Eds.), Proceedings of the Gulf of Maine Ecosystem Dynamics Scientific Symposium and Workshop. Regional Association for Research in the Gulf of Maine, pp. 39–52.
- Bigelow, H.B., 1927. Physical oceanography of the Gulf of Maine. *Fish. Bull.* 40, 511–1027.
- Brooks, D.A., 1985. The vernal circulation in the Gulf of Maine. *J. Geophys. Res.* 90, 4687–4705.
- Churchill, J.H., Pettigrew, N.R., Signell, R.P., 2005. Structure and variability of the Western Maine Coastal Current. *Deep-Sea Res Part II* 52 (19–21), 2392–2410.
- Fletcher, R.A., 1976. A tidal model of the northwest European continental shelf. *Mem. Soc. R. Sci. Liege* 6 (10), 141–164.
- Haidvogel, D.B., Arango, H., Budgell, W.P., Cornuelle, B.D., Curchitser, E., Di Lorenzo, E., Fennel, K., Geyer, W.R., Hermann, A.J., Lanerolle, L., Levin, J., McWilliams, J.C., Miller, A.J., Moore, A.M., Powell, T.M., Shchepetkin, A.F., Sherwood, C.R., Signell, R.P., Warner, J.C., Wilkin, J., 2008. Ocean forecasting in terrain-following coordinates: formulation and skill assessment of the Regional Ocean Modeling System. *J. Comput. Phys.* 227 (17), 3595–3624.
- Hannah, C.G., Naimie, C.E., Loder, J.W., Werner, F.E., 1998. Upper-ocean transport mechanisms from the Gulf of Maine to Georges Bank, with implications for calanus supply. *Cont. Shelf Res.* 17 (15), 1887–1911.
- He, R., Weisberg, R.H., 2003. West Florida shelf circulation and temperature budget for the 1998 fall transition. *Cont. Shelf Res.* 23, 777–800.
- He, R., McGillicuddy, D.J., Lynch, D.R., Smith, K.W., Stock, C.A., Manning, J.P., 2005. Data assimilative hindcast of the Gulf of Maine coastal circulation. *J. Geophys. Res.* 110, C10011, <http://dx.doi.org/10.1029/2004JC002807>.
- He, R., McGillicuddy, D., 2008. Gulf of Maine Harmful Algal Bloom in Summer 2005: part 1. In-situ observations of coastal hydrography and circulation. *J. Geophys. Res.* 113, C07039, <http://dx.doi.org/10.1029/2007JC004691>.
- He, R., McGillicuddy, D., Anderson, D., Keafer, B., 2008. Gulf of Maine circulation and harmful algal bloom in summer 2005: part 2: bio-physical numerical modeling. *Journal of Geophysical Research: Oceans* 113, C07040, <http://dx.doi.org/10.1029/2007JC004602>.
- Incze, L., Xue, H., Wolff, N., Xu, D., Wilson, C., Steneck, R., Wahle, R., Lawton, P., Pettigrew, N., Chen, Y., 2010. Connectivity of lobster (*Homarus americanus*) populations in the coastal Gulf of Maine: part II. Coupled biophysical dynamics. *Fish. Oceanogr.* 19, 1–20, <http://dx.doi.org/10.1111/j.1365-2419.2009.00522.x>.
- Li, Y., He, R., McGillicuddy, D., Anderson, D., Keafer, B., 2009. Investigation of 2006 *Alexandrium fundyense* bloom in the Gulf of Maine: in situ observations and numerical modeling. *Cont. Shelf Res.*, <http://dx.doi.org/10.1016/j.csr.2009.07.012>.
- Luettich, R.A., Muccino, J.C., Foreman, M.G.G., 2002. Considerations in the calculation of vertical velocity in three-dimensional circulation models. *J. Atmos. Oceanic Technol.* 19, 2063–2076.
- Lynch, D.R., Holboke, M.J., Naimie, C.E., 1997. The Maine coastal current: Spring climatological circulation. *Cont. Shelf Res.* 17 (6), 605–634.
- Manning, J.P., Churchill, J.H., 2006. Estimates of dispersion from clustered-drifter deployments on the southern flank of Georges Bank. *Deep-Sea Res. II* 53, 2501–2519.
- Manning, J.P., McGillicuddy, D.J., Pettigrew, N.R., Churchill, J.H., Incze, L.S., 2009. Drifter observations of the Gulf of Maine coastal current. *Cont. Shelf Res.* 29 (7), 835–845, doi:10.1016/j.csr.2008.12.008.
- Marchesiello, P., McWilliams, J.C., Shchepetkin, A.F., 2001. Open boundary conditions for long-term integration of regional oceanic models. *Ocean Model.* 3, 1–20.
- McGillicuddy, D.J., Signell, R.P., Stock, C.A., Keafer, B.A., Keller, M.D., Hetland, R.D., Anderson, D.M., 2003. A mechanism for offshore initiation of harmful algal blooms in the coastal Gulf of Maine. *J. Plankton Res.* 25 (9), 1131–1138.
- McGillicuddy, D.J., Anderson, D.M., Lynch, D.R., Townsend, D.W., 2005a. Mechanisms regulating the large-scale seasonal fluctuations in *Alexandrium fundyense* populations in the Gulf of Maine: results from a physical–biological model. *Deep-Sea Res. II* 52, 2698–2714.
- McGillicuddy, D.J., Anderson, D.M., Solow, A.R., Townsend, D.W., 2005b. Inter-annual variability of *Alexandrium fundyense* abundance and shellfish toxicity in the Gulf of Maine. *Deep-Sea Res. II* 52, 2843–2855.
- McGillicuddy, D.J., Townsend, D.W., He, R., Keafer, B.A., Kleindinst, J.L., Li, Y., Manning, J.P., Mountain, D.G., Thomas, M.A., Anderson, D.M., 2011. Suppression of the 2010 *Alexandrium fundyense* bloom by changes in physical, biological, and chemical properties of the Gulf of Maine. *Limnol. Oceanogr.* 56 (6), 2411–2426.
- McGillicuddy, D.J., Brosnahan, M.L., Couture, D.A., He, R., Keafer, B.A., Manning, J.P., Martin, J.L., Pilskaln, C.H., Townsend, D.W., Anderson, D.M., 2014. A red tide of *Alexandrium fundyense* in the Gulf of Maine. *Deep-Sea Res. II* 103, 174–184.
- Mellor, L.G., Yamada, T., 1982. Development of a turbulence closure model for geophysical fluid problems. *Rev. Geophys. Space Phys.* 20 (4), 851–875.
- Mitarai, S., Siegel, D.A., Watson, J.R., Dong, C., McWilliams, J.C., 2009. Quantifying connectivity in the coastal ocean with application to the Southern California Bight. *J. Geophys. Res.* 114, C10026, <http://dx.doi.org/10.1029/2008JC005166>.
- Moody, J.A., et al., 1984. Atlas of tidal elevation and current observations on the Northeast American continental shelf and slope. *US Geol. Surv. Bull.* 1611, 122.
- North, E.W., Hood, R.R., Chao, S.-Y., Sanford, L.P., 2006a. Using a random displacement model to simulate turbulent particle motion in a baroclinic frontal zone: a new implementation scheme and model performance tests. *J. Mar. Syst.* 60, 365–380.
- North, E.W., Z. Schlag, R.R. Hood, L. Zhong, M. Li, T. Gross, 2006b. Modeling Dispersal of *Crassostrea ariakensis* Oyster Larvae in Chesapeake Bay. Final Report to Maryland Department of Natural Resources, July 31, 2006, 55 p.
- North, E.W., Schlag, Z., Hood, R.R., Li, M., Zhong, L., Gross, T., Kennedy, V.S., 2008. Vertical swimming behavior influences the dispersal of simulated oyster larvae in a coupled particle-tracking and hydrodynamic model of Chesapeake Bay. *Mar. Ecol. Prog. Ser.* 359, 99–115.

- Schlag, Z., E.W. North, K. Smith, 2008. Larval TRANSport Lagrangian model (LTRANS) User's Guide. University of Maryland Center for Environmental Science, Horn Point Laboratory, Cambridge, MD, 146 pp.
- Pettigrew, N.R., Churchill, J.H., Janzen, C.D., Mangum, L.J., Signell, R.P., Thomas, A.C., Townsend, D.W., Wallinga, J.P., Xue, H., 2005. The kinematic and hydrographic structure of the Gulf of Maine coastal current. *Deep-Sea Res. Part II* 52 (19–21), 2369–2391.
- Pettigrew, N.R., Fleming, R.J., Fikes, C.P., 2011. The history of the first decade of the observing system in the Gulf of Maine, and plans for the second decade. *MTS Journal* 2011, 1–10.
- Shchepetkin, A.F., McWilliams, J.C., 2005. The regional ocean modeling system (ROMS): a split-explicit, free-surface, topography-following coordinates ocean model. *Ocean Model.* 9 (4), 347–404.
- Xue, H., Chai, F., Pettigrew, N.R., 2000. A model study of seasonal circulation in the Gulf of Maine. *J. Phys. Oceanogr.* 30, 1111–1135.
- Xue, H., Incze, L., Xu, D., Wolff, N., Pettigrew, N., 2008. Connectivity of lobster populations in the coastal Gulf of Maine, Part I: Circulation and larval transport potential. *Ecol. Model.* 210, 193–211.